

Conformational plasticity of the ULK3 kinase domain

Sebastian Mathea^{1,2#*}, Eidarus Salah^{3,4*}, Cynthia Tallant^{3,4}, Deep Chatterjee^{1,2}, Benedict-Tilman Berger^{1,2},
Rebecca Konietzny⁴, Susanne Müller², Benedikt M Kessler⁴ and Stefan Knapp^{1,2,5#}

¹Institute of Pharmaceutical Chemistry, Goethe-University Frankfurt, 60438 Frankfurt, Germany

²Structural Genomics Consortium (SGC), Buchmann Institute for Life Sciences, Goethe-University Frankfurt, 60438 Frankfurt, Germany

³Structural Genomics Consortium (SGC), Nuffield Department of Medicine, University of Oxford, Oxford, OX37DQ, UK

⁴Target Discovery Institute (TDI), Centre for Medicines Discovery, Nuffield Department of Medicine, University of Oxford, Oxford, OX37FZ, UK

⁵German Cancer Network (DKTK), Frankfurt/Mainz, 60438 Frankfurt, Germany

***These authors contributed equally to the work.**

#To whom correspondence should be addressed

Sebastian Mathea

Email: mathea@pharmchem.uni-frankfurt.de

Stefan Knapp

Email: knapp@pharmchem.uni-frankfurt.de

Abstract

The human protein kinase ULK3 regulates the timing of membrane abscission, thus being involved in exosome budding and cytokinesis. Herein, we present the first high-resolution structures of the ULK3 kinase domain. Its unique features are explored against the background of other ULK kinases. An inhibitor fingerprint indicates that ULK3 is highly druggable and capable of adopting a wide range of conformations. In accordance with this, we describe a conformational switch between the active and an inactive ULK3 conformation, controlled by the properties of the attached small-molecule binder. Finally, we discuss a potential substrate-recognition mechanism of the full-length ULK3 protein.

Introduction

Membrane abscission is the ultimate step in several physiologically important processes such as exosome budding and cytokinesis.¹ Any connection between two membrane substructures is cut, setting free extracellular vesicles or two separated daughter cells. In contrast to clathrin-coated vesicles, which are shed by dynamins, abscission in exosome budding and cytokinesis is mediated by the **Endosomal Sorting Complexes Required for Transport (ESCRT)** machinery. This is basically a compilation of cytosolic protein complexes for membrane binding, membrane bending and membrane severing.¹

The membrane patches that are destined for abscission are primed with adaptor proteins such as charged multivesicular body protein 7 (CHMP7) or centrosomal protein of 55 kDa (CEP55).² The priming is enhanced by ubiquitination of transmembrane proteins. These factors contribute to recruiting early ESCRT complexes, namely the ESCRT-I, ESCRT-II or ALIX complexes, which in turn form nucleation sites for the growth of the polymeric ESCRT-III complex.² The ESCRT-III complex is made up of several hundred CHMP and IST1 molecules, associated to form spirals of membrane-bound filaments that define the membrane curvature.³ CHMP proteins contain an α -helical polymerisation domain and a C-terminal MIT interacting motif (MIM). Structural studies have shown that the polymerisation domain toggles between a globular conformation in solution and an extended conformation in the ESCRT-III complex.³ The MIM helices are attached to the polymerization domain via a flexible linker and are recognized by microtubule interacting and transport (MIT) domains. Examples for MIT domain containing proteins are vacuolar protein sorting-associated protein 4A (VPS4A), a AAA ATPase that promotes ESCRT-III disassembly, and unc-51-like kinase 3 (ULK3), the protein this article is focused on.⁴

Besides its tandem MIT domain, ULK3 also contains a Ser/Thr-kinase domain (**Figure 1A**). ULK3 was shown to catalyse the phosphorylation of the ESCRT-III proteins CHMP1A/B, CHMP2A and IST1 both *in vitro* and *in situ*.⁴ This phosphorylation changes the subcellular localization of ESCRT-III building blocks and prevents their polymerisation. Thereby, catalytically active ULK3 delays abscission as the final step of cytokinesis and contributes to a more stringent abscission checkpoint.⁴

ULK3 is part of a small kinase subfamily. Five ULKs are expressed in humans and higher eukaryotes: ULK1 to ULK4 and STK36.⁵ ULK subfamily members are thought to have emerged during evolution from subsequent gene duplications, the sequence identities of the kinase domains range from 29% to 79% (**Figure 1A**). In addition to their N-terminal kinase domain, the ULKs comprise various domains assumed to mediate protein interactions. In ULK1 and ULK2, the C-terminal domain (CTD)-like domain is essential for the recruitment of the autophagy-related protein 13 (ATG13).⁶ This domain is replaced in ULK3 with the aforementioned MIT domain tandem, while ULK4 and STK36 both contain C-terminal armadillo repeat domains (**Figure 1A**).

ULK1 was the first subfamily member to be described⁷, since then this isoform has been subjected to intense research. It has been found to be a key regulator of autophagy, in that it links nutrient sensing by the mammalian target of rapamycin complex 1 (mTORC1) to the induction of the early autophagosome, a complex of ULK1 and its binding partners ATG13, ATG101 and FIP200.⁸ This complex initiates autophagy, a survival mechanism comprising the orderly degradation of cellular components. ULK1 and the homologous ULK2 are thereby linked to the development of human diseases such as tumorigenesis⁹ and neurodegeneration¹⁰.

In addition to modulating the timing of membrane abscission, ULK3 was suggested to play a role in several signalling pathways. Though it is not required for autophagy induced by low nutrient levels, studies on the *Drosophila* ULK3 ortholog Another drosophila Unc-51-like kinase (ADUK) demonstrated its requirement for autophagy induced by chemical stress.¹¹ In human fibroblasts, overexpression of ULK3 induced autophagy and senescence, suggesting that the role of ULK3 in stress-induced autophagy is conserved from fly to man.¹² ULK3 has also been described as a regulator of hedgehog signalling by binding to the suppressor of fused (Sufu), a protein required for negative regulation of GLI proteins.¹³ Furthermore, ULK3 was reported to directly phosphorylate GLI2.¹⁴ In genome-wide association studies (GWAS), genetic alterations in ULK3 have been linked to blood pressure and hypertension^{15, 16} and mood states¹⁷.

To date, eight high-resolution structure models of the related ULK1/2 kinase domains have been made available in the PDB.¹⁸⁻²¹ All of them are similar in that the kinase domains adopt the canonical active-like conformation, and in that a broad-specificity type-1 inhibitor is bound in the active site.¹⁸⁻²¹ Notably, nothing is known about ULK1/2 plasticity and about possible inactive conformations. In contrast to the other ULK subfamily members, ULK4 is a pseudokinase. Several sequence motifs that are typically found in kinases and that are indispensable for catalytic activity are not conserved in ULK4. Two ULK4 structure models have recently been published, one showing ULK4 in complex with its physiological cofactor ATP²², and one in complex with a low-affinity inhibitor²³. Again, there is no indication for domain plasticity – ATP binds tightly to the pseudoactive site and condenses ULK4 as also shown in MD simulations.²²

In contrast, structural information on the ULK3 and STK36 kinase domains is still lacking. The understanding of their complex functional roles both in physiology and in pathophysiology will be aided by high-resolution structure models that provide insight into their regulation as well as by selective chemical probes that can be used in cellular model systems or *in vivo* to study ULK function.^{24, 25} Here, we report screening data of ULK3 against a set of clinical kinase inhibitors as well as crystal structures of ULK3 in complex with type-1 and type-2 inhibitors providing a basis for the rational development of more selective ULK3 inhibitors targeting the active as well as the inactive state. Due to the diverse functions of ULK3 in membrane

abscission, stress induced autophagy as well as regulation of hedgehog signalling, selective chemical probes will represent valuable tools for the exploitation of this interesting kinase as a potential drug target.

Methods

Cloning. The DNA coding for a His₆-tag, a TEV cleavage site and the ULK3 residues 2 to 277 was synthesised (Genscript, **Figure S1**) and cloned into the expression vector pET-28a, using the NcoI and XhoI restriction sites. The plasmids for ULK1₁₋₂₈₃ expression¹⁹ and ULK2₁₋₂₇₇ expression²⁰ were kind gifts from Kevan Shokat's group at UCSF.

Expression and purification. The respective expression plasmid was transformed into BL21(DE3) Competent *E. coli* (NEB), and expression was performed as previously described²⁶. For ULK3₂₋₂₇₇ purification, bacteria were then resuspended in lysis buffer (50 mM HEPES pH 7.4, 500 mM NaCl, 20 mM imidazole, 0.5 mM TCEP, 5% glycerol) and lysed by three passages through the high-pressure cell breaker. The lysate was cleared by centrifugation and loaded onto a Ni NTA column. After vigorous rinsing with lysis buffer, the His₆-tagged protein was eluted in lysis buffer containing 300 mM imidazole. While the protein was subjected to dialysis to remove the imidazole, the N-terminal tag was cleaved by TEV protease. Contaminating proteins, the cleaved tag and TEV protease were removed by another Ni NTA step. Finally, ULK3₂₋₂₇₇ was concentrated and subjected to gel filtration using an AKTA Xpress system combined with a HiLoad 16/600 Superdex 200 pg gel filtration column. The elution volume 94.4 mL indicated the protein to be monomeric in solution. The final yield was 15 mg ULK3₂₋₂₇₇/L TB medium. ULK1₁₋₂₈₃ purification¹⁹ and ULK2₁₋₂₇₇ purification²⁰ was performed as previously described.

Differential scanning fluorimetry (DSF). The assay was performed according to a previously established protocol.²⁷ Briefly, a solution of 2 μ M ULK protein in assay buffer (20 mM HEPES pH 7.4, 150 mM NaCl, 0.5 mM TCEP, 5% glycerol) was mixed 1:1000 with SYPRO Orange (Sigma). The compounds to be tested were added to a final concentration of 10 μ M. 20 μ L of each sample were placed in a 96-well plate and heated gradually from 25°C to 96°C. Fluorescence was monitored using an Mx3005P real-time PCR instrument (Stratagene) with excitation and emission filters set to 465 and 590 nm, respectively. Data was analysed with the MxPro software.

Isothermal titration calorimetry (ITC). Measurements were performed at 20°C on a MicroCal VP-ITC (GE Healthcare). ULK3₂₋₂₇₇ was dialysed overnight into assay buffer (20 mM HEPES pH 7.5, 300 mM NaCl, 0.5 mM TCEP). The syringe was loaded with 87 μ M ULK3₂₋₂₇₇, the cell was filled with assay buffer containing 8 μ M of the respective inhibitor. Every 5 minutes, 10 μ L of the protein solution was injected into the cell for a total of 29 injections. The heat flow data was analysed with the MicroCal ORIGIN software package employing a single binding site model.

Crystallisation of the ULK3-bosutinib complex. 100 nL of a solution containing the protein-ligand complex (20 mg/mL ULK3₂₋₂₇₇, 500 μ M bosutinib) were transferred to a 3-well crystallisation plate (Swissci), mixed with 50 nL precipitant solution (0.1 M Tris pH 8.5, 0.2 M sodium citrate, 30% PEG400) and incubated at 4°C. Crystals appeared after 12 days and did not change appearance after 24 days. They were mounted in precipitant solution cryoprotected with additional 25% ethylene glycol. Data was collected at Diamond Light Source, analysed, scaled and merged with Xia2²⁸. The structure was solved by molecular replacement with Phaser²⁹ using a ULK1 model as a template (PDB ID 4WNP) and refined with Refmac5³⁰. The model was validated using MolProbity³¹. The model and the structure factors have been deposited to the PDB with the ID 6FDY (crystallographic parameters in **Table S1**).

Crystallisation of the ULK3-momelotinib complex. 100 nL of a solution containing the protein-ligand complex (15 mg/mL ULK3₂₋₂₇₇, 500 μ M momelotinib) were transferred to a 3-well crystallisation plate (Swissci), mixed with 50 nL precipitant solution (0.1 M HEPES pH 7.5, 0.2 M MgCl₂, 30% 2-propanol) and incubated at 4°C. Crystals appeared after 1 day and did not change appearance after 4 days. Data collection and analysis was performed as described above. Model and structure factors have been deposited to the PDB with the ID 6FDZ (crystallographic parameters in **Table S1**).

ULK3₂₋₂₇₇ phosphomapping. 100 μ L of a ULK3₂₋₂₇₇ solution (50 μ M) were mixed with 100 μ L of an ATP/Mg²⁺ solution (2 mM ATP, 5 mM MgCl₂). The reaction mixture was incubated at 37°C for 30 minutes to allow for autophosphorylation. Following this, the ULK3 protein was subjected to methanol/chloroform precipitation, digestion with elastase and analysis by liquid chromatography tandem mass spectrometry (LC-MS/MS) as described previously.³²

Results

The ULK3 sequence indicates an active protein kinase. The kinase domain in the ULK3 N terminus contains all 5 conserved kinase motifs necessary for catalytic activity, but with a number of minor sequence variations: In the glycine-rich loop, one of the conserved glycine residues is exchanged for an alanine in ULK3. While the VAIK motif in the β 3 strand is intact, the HRD motif is altered to HLD in ULK3, importantly still harbouring the catalytic aspartate. Also present are the asparagine in +5 position from the HRD and, finally, the DFG motif in the base of the activation segment (**Figure 1B**). The ULK3 secondary structure elements (predicted with the PSIPRED online tool³³) corresponded perfectly to the well-known kinase topology. In the human kinome, ULK1 is the closest homolog of ULK3. Both kinase domains share a sequence identity of 40%. The most obvious difference is a 7 amino acid insertion in the loop connecting the β 7 and β 8 strands that is only present in ULK1. Interestingly, the ULK1 and ULK3 activation loops share no sequence similarity whatsoever. Even potential phosphorylation sites are shuffled, indicating different

regulation mechanisms for ULK1 and ULK3. Striking sequence variability is also observed in the α G helices of both kinases. On top of this variability, the position of the ULK3 α G helix is shifted by two residues compared to ULK1 (**Figure 1B**).

Producing the recombinant ULK3 kinase domain. The ULK3 residues 2 to 277 covered the kinase domain as estimated from comparison with ULK1. However, the expression of ULK3₂₋₂₇₇ in *E. coli* led to highly phosphorylated protein, indicating the ULK3 kinase to be catalytically active even without priming phosphorylations and accessory factors. Due to the phosphorylations at multiple and most likely random sites during expression, the protein was unstable, and we were unable to purify it to homogeneity. The co-expression of λ phosphatase allowed for the expression of non-phosphorylated ULK3₂₋₂₇₇. In contrast to the protein expressed in absence of λ phosphatase, this protein was stable even at high protein concentrations and turned out to be suitable both for structural work and for inhibitor binding studies. As references, the ULK1 and ULK2 kinase domains were expressed and purified as described in recent publications.^{19, 20}

Structure of the ULK3 active state. To gain insight into the ULK3 regulatory mechanism, and to explore how to target the ULK3 kinase domain with small-molecule binders, we determined the 3D structure of ULK3 in complex with a tight-binding reversible inhibitor (the identification of bosutinib as ULK3 inhibitor will be discussed in a later section). As expected, ULK3 presented the canonical bilobal kinase fold, with the inhibitor occupying the cleft between the two lobes (**Figure 1D**). In active kinases, several core residues assemble into an internal scaffolding network referred to as hydrophobic spines.³⁴ As a consequence of this three-dimensional alignment, the active site residues are oriented for catalysis. In ULK3, both the catalytic and the regulatory spine were fully assembled. The catalytic spine comprised (top to bottom) A42 from the VAIK motif, the inhibitor's aromatic hinge binder instead of the ATP purine rings, L144 and I143 from the β 7 strand and, finally, I202 that mounted the spine to the rigid α F helix. The regulatory spine contained (again top to bottom) L77 from the α C β 4 loop, L66 from the α C helix, F158 from the DFG motif and H135 from the HRD motif (**Figure 1D**). Another kinase feature that is linked to activity regulation is the activation loop. For many kinases, a phosphorylated activation loop is firmly attached to the kinase C lobe and serves as a docking site for potential protein substrates, while a non-phosphorylated activation loop is more flexible and restricts the access of potential protein substrates to the active site. Thereby, activation loop phosphorylation switches the kinase from its enzymatically inactive to its active form.³⁵ The ULK3 activation loop was not phosphorylated. Nevertheless, it was firmly attached to the ULK3 C lobe. It is worth mentioning that the electron density of the activation loop was clearly defined, and that its B factors were similar to the average B factors of the kinase domain. While the kinase core with the intact spines and the attached activation loop indicated an active kinase conformation, the K-E salt bridge that usually anchors the α C helix to the β 3 strand in active kinases was not formed. However, the K44 to E62 distance of 7.0 Å resulted mainly from the inhibitor displacing the K44 side chain and pushing it away from E62.

Comparison of the ULK3 and ULK1 catalytic domains. Though both kinase domains share only 40% sequence identity, their overall 3D appearances were remarkably similar (PDB ID 5CI7¹⁹, **Figure 1C**). The RMSD value between all C α atoms was 2.4 Å. A striking difference was observed in the β 3 α C linker that was extended in ULK3. This might allow the ULK3 α C helix to adopt more pronounced out conformations. And as already spotted in the sequence alignment (**Figure 1B**), the insertion between the β 7 and β 8 strands contained additional residues in ULK1. The functional consequence of this insertion was, however, not obvious. Surprisingly, the ULK1 and ULK3 activation loops adopted identical conformations despite their very different primary sequences. We concluded that this particular activation loop conformation is conserved in ULK1 and ULK3, but the mechanisms to stabilize and to destabilize it differ between the two kinases. Finally, the orientations of the α G helices varied substantially. While the ULK1 α G helix was rather attached to the C lobe, the ULK3 α G helix pointed outwards. Thereby, they likely formed distinct docking sites for their respective sets of protein substrates. These observations highlighted once again that despite all similarities, even closely related kinases can differ in activity regulation and substrate recognition.

ULK3 is a highly druggable kinase target. In order to identify chemical starting points for the development of ULK3 binders, we screened a library of clinical and pre-clinical kinase inhibitors (purchased from Selleckchem, **Table S2**). We performed differential scanning fluorimetry (DSF) assay, a versatile method to determine the temperature at which a given protein denatures from heat. Tight binding of a small molecule generally stabilizes the protein thus leading to a higher melting temperature (T_M). Notably, kinases are particularly sensitive to this assay format.³⁶ In addition to the ULK3 kinase domain, we also tested the homologous ULK1 and ULK2 kinase domains for comparison. In the absence of inhibitors, the melting temperatures of the three proteins were similar, with ULK1 (46°C) being slightly less stable than ULK2 and ULK3 (both 49°C). As expected, some of the tested compounds stabilized the ULK proteins, a list of all compounds with the corresponding T_M shifts is given in **Table S2**. Out of 150 compounds, 7 compounds increased ULK1 T_M by >8 K. For ULK2, it was only 3 compounds, and 10 compounds were identified for ULK3, suggesting excellent druggability. The best hit for ULK1 and ULK2 was dabrafenib (with a ΔT_M of 12 and 11 K, respectively) in line with recent potent inhibitors that have been developed for this target³⁷ sharing the aminopyrimidine hinge binding motif. For ULK3, the most potent hit was the pan-FGFR inhibitor LY2874455³⁸ (ΔT_M of 13 K). ULK1 and ULK2 were stabilized by a similar set of compounds, while the stabilization patterns for ULK1 and ULK3 differed substantially (the cross-correlations of the T_M shifts are depicted in **Figure 2A**). In terms of isoform specificity, the compounds foretinib and SU6668 stood out. Foretinib, a broad-spectrum tyrosine kinase inhibitor, stabilized ULK3 by 11 K, but ULK1/2 only by <4 K suggesting that ULK3 differs from the other ULK family members by accommodating this bulky type-2 kinase inhibitor. The oxindole SU6668 (orantinib), that was previously reported to inhibit ULK3³⁹, was confirmed in our screen. It stabilized ULK3 by 8.6 K, but ULK1/2 only by <2 K. Taken together, this demonstrated that ULK3 inhibitors without cross reactivity towards the other ULK proteins can be

developed (**Figure 2C**). Interestingly, ULK3 was stabilized by both type-1 kinase inhibitors (such as lestaurtinib and bosutinib) and type-2 inhibitors (such as foretinib and momelotinib). In contrast, only weaker interactions with type-2 inhibitors were observed for ULK1/2 suggesting that the DFG-out conformation is less favoured in these kinases.

Hit validation with isothermal titration calorimetry (ITC). Since DSF results do not only depend on affinity, but also on the respective inhibitor binding mode and on the stability of the apo protein, we confirmed inhibitor binding affinity with an orthogonal assay. We employed ITC with the identified inhibitors foretinib, SU6668, bosutinib and momelotinib (**Figure 2B**). The binding of foretinib to the ULK3 kinase was characterized by a dissociation constant (K_D) of 20 nM. The binding was enthalpically driven ($\Delta H = -7.3 \text{ kcal}\cdot\text{mol}^{-1}$) with a substantial entropic contribution to binding ($-T\Delta S = -3.0 \text{ kcal}\cdot\text{mol}^{-1}$). The affinity of bosutinib to ULK3 was lower ($K_D = 48 \text{ nM}$). This was in good agreement with the DSF results. In comparison to foretinib, bosutinib binding was more entropically driven ($-T\Delta S = -6.2 \text{ kcal}\cdot\text{mol}^{-1}$), with a significant enthalpic contribution ($\Delta H = -3.6 \text{ kcal}\cdot\text{mol}^{-1}$). The ITC titrations for SU6668 and momelotinib were noisy (data not shown) and thus not suitable for calculation of binding constants and thermodynamic parameters. This was most likely due to poor compound solubility. A comparison of DSF and ITC results is shown in **Figure 2C**.

Bosutinib binding mode to ULK3. The BCR-ABL inhibitor bosutinib was identified as a ULK3 kinase binder in DSF assay and confirmed by ITC. The active-like ULK3 structure described above (**Figure 1D**) was obtained by co-crystallization of ULK3 and bosutinib. The inhibitor was ATP competitive, occupying the solvent exposed front pocket (**Figure 3A**), in a similar fashion to what was observed with the tyrosine kinase ABL⁴⁰. Bosutinib was bound as a type-1 inhibitor with the base of the ULK3 activation segment in the DFG-in conformation. The quinoline nitrogen formed a hydrogen bond with the backbone of C94 in the ULK3 hinge. The other interactions were exclusively mediated by the substituents of the bosutinib benzene ring: the *ortho*-chlorine to the backbone of A42 in the $\beta 3$ sheet, the *para*-chlorine to D157 in the DFG motif, and the methoxy group to the conserved N142 prior to the $\beta 7$ sheet (**Figure 3A**). Notably, bosutinib binding prevented the K44 E62 salt bridge from being formed, mainly by displacing the K44 side chain.

Momelotinib binding induces the DFG-out conformation. All DSF hits with $\Delta T_M > 6 \text{ K}$ were probed in ULK3 co-crystallization studies. Of these, only momelotinib led to crystals with satisfying diffraction properties (resolution $< 3 \text{ \AA}$). Momelotinib was originally developed to target JAK1/2. In our structure model, it bound to ULK3 as a type-2 inhibitor with the base of the activation segment in the DFG-out conformation, but without occupying the DFG-out allosteric pocket (**Figure 3B**). Instead, one of the momelotinib biphenyl rings recruited the DFG F158 sidechain to form a π -stacking interaction thus stabilizing the DFG-out conformation. Similar to bosutinib, momelotinib was anchored via a hydrogen bond to the C94 backbone in the ULK3 hinge. We also observed its nitrile pointing towards the ULK3 glycine-rich loop and interacting with G23 and A26 backbone atoms. And finally, the momelotinib amide oxygen tightly bound the conserved

K44 in the $\beta 3$ sheet, providing additional stability to the complex (**Figure 3B**). We are not aware of any other structure model showing momelotinib bound to a kinase. XL019, a compound that resembles momelotinib, has high selectivity for JAK2, but unlike momelotinib, it stabilized its protein target in the DFG-in conformation.⁴¹ The surprising binding mode and its favourable kinome-wide selectivity make momelotinib an interesting starting point for the development of a ULK3 chemical probe. One possible strategy is here to exploit the pocket resulting from the DFG-flip that is likely not present in other momelotinib targets. Another option is to merge bosutinib and momelotinib features in one molecule to obtain inhibitors with improved affinity and selectivity.

Structural flexibility in the ULK3 kinase domain. Our diverse ULK3-inhibitor complexes revealed the ULK3 propensity to undergo substantial conformational changes. When bosutinib was bound, the kinase domain adopted an active-like α C-in DFG-in conformation. Both E62 from the α C helix and D157 from the DFG motif pointed towards the ATP binding site. Furthermore, the activation loop was firmly attached to the kinase C lobe, and the regulatory spine was fully assembled (**Figure 4A**). In contrast, when momelotinib was bound, the α C helix was rotated outwards by 45°, and the DFG F158 was flipped out of its hydrophobic pocket to form a π -stacking interaction with the inhibitor. In this inactive α C-out DFG-out conformation, neither E62 nor D157 were close to the ATP binding site. The activation segment was not attached to the C-lobe but it occupied the space vacated by the displaced α C helix. As a consequence of all these structural rearrangements, the regulatory spine was completely broken (**Figure 4B**). In addition to their role as enzymes, kinases can also function as scaffolds and allosteric modulators. If this is the case for ULK3, our differentially binding inhibitors are expected to have a differential impact on non-catalytic ULK3 signalling.

The ULK3 kinase is constitutively active. Regulation of kinase activity by activation loop phosphorylation is a common theme in protein kinases.³⁵ Accordingly, autophosphorylation of the activation loop residue T180 boosts the kinase activity of the ULK3 homolog ULK1.¹⁹ The regulatory mechanism for ULK3 is different though. In order to identify potential autophosphorylation sites, we incubated unphosphorylated ULK3₂₋₂₇₇ with ATP/Mg²⁺ for 30 minutes at 37°C, followed by elastase digestion and LC-MS/MS analysis (**Figure S2**). We found that ULK3 was heavily autophosphorylated with all 10 phosphosites being located in flexible loop regions on the surface of the protein, such as S55 in the $\beta 3$ α C linker, S146 in the $\beta 7$ $\beta 8$ insert and S215 in the α F α G loop (**Figure 4C**). There was no indication any of these phosphosites were physiologically relevant. The activation loop, however, was spared from the *in vitro* autophosphorylation. We concluded that ULK3 possessed constitutive kinase activity even in its unphosphorylated form. This observation is also supported by the ULK3-bosutinib structure model. The unphosphorylated activation loop was firmly attached to the kinase C lobe, the lack of a stabilizing phosphoresidue was compensated for by an unusual salt bridge (Q162 to R174, **Figure 4D**). Taken together, we conclude that the activation loop conformation is conserved between ULK1 and ULK3, but the regulatory mechanism is not. However, these

observations concern the kinase domain only. In the full-length ULK3, there are additional levels of activity regulation, also linked to substrate recognition.

Modelling of the ULK3-IST1 complex. Several proteins have been described as cellular ULK3 kinase substrates.^{4, 14} A particularly compelling substrate recognition mechanism can be hypothesized for the ESCRT-III component IST1: ULK3 bears two MIT domains in its C terminus, while IST1 contains two MIT interacting motifs (MIMs). The binding of the second MIM to the second MIT domain was demonstrated experimentally⁴, furthermore, the binding of both IST1 MIMs to the ULK3 MIT tandem is sterically possible. This binding mode places the IST1 polymerization domain next to the ULK3 kinase domain. The interaction of ULK3 and IST1 was modelled and refined using a simple molecular dynamics tool (phenix.dynamics⁴²). In the resulting model, the ULK3 activation loop and α G helix served as docking patch for the IST1 polymerization domain, and the IST1 phosphoacceptor residue S152 was in close proximity to the ULK3 active site (**Figure 4E**). According to this substrate-recognition mechanism, the cellular ULK3 might be localized to regions of high ESCRT-III activity, scanning for free MIMs, and phosphorylating the CHMP and IST1 polymerization domains.⁴ Like this, free CHMP and IST1 are silenced, resulting in a more stringent abscission checkpoint.

Discussion

Domain plasticity is a well-established concept in the kinase field.⁴³ Its fundamental principle is that kinases toggle between an active conformation, which is very similar in all kinases, and one or several inactive conformations, which can differ substantially between individual kinases. In general, the kinase structural elements with the highest degree of freedom are the glycine-rich loop, the α C helix and the activation loop including the DFG motif in its base. All these elements are highly dynamic in ULK3, establishing ULK3 as an interesting example for a kinase with pronounced domain plasticity. In addition to the active-like ULK3 conformation, we observed a DFG-out α C-out inactive conformation. Importantly, we have identified small-molecule binders that trap ULK3 in either the active-like (such as SU6668 and bosutinib) or the inactive conformation (such as foretinib and momelotinib). In solution, we expect the ULK3 kinase domain to adopt an ensemble of diverse conformations. The secondary structure elements are formed also in the apo protein as confirmed with circular dichroism (CD) spectroscopy (**Figure S3**). When adding an inhibitor, one particular conformation is stabilized. Accordingly, our crystal structures provide two of many possible snapshots of the ULK3 kinase domain in solution. At this point, we can only speculate about the atomistic mechanism by which the active-like ULK3 conformation transforms into the inactive conformation. Likely, the mechanism is initiated by rotating out the α C helix to creating space for the DFG-flip and the HRD-flip as observed for other kinases.^{44, 45} An important question here is whether there are stable intermediates that possibly can be targeted by yet to discover inhibitors. These hypothetical intermediates might involve a

folded activation loop as described for Bruton's tyrosine kinase (BTK)⁴⁴ or the DFG-up conformation as described for Aurora kinase B (AURKB)⁴⁵.

Until now, structural data on the ULK3 full-length protein is elusive. Either the kinase and C-terminal MIT1/2 domains act as pearls-on-a-string, with the MIT1/2 domains just fishing for potential substrates, or they contribute to stabilizing the inactive kinase conformation as autoinhibitory domains. As mentioned above, active ULK3 modulates the timing of membrane abscission, resulting in a more stringent abscission checkpoint.⁴ The spatiotemporal regulation of ULK3 activity is therefore expected to be tight. However, the cellular determinants of this regulation are so far unknown: ULK3 might be the client of an allosteric protein binder that stabilizes one specific ULK3 conformation. There is also the possibility of ULK3 post-translational modifications (PTMs) we are not aware of at this point. And finally, the binding of a physiological substrate such as monomeric IST1 (**Figure 4E**) might induce and stabilize the active ULK3 conformation and trigger phosphorylation. Thus, only monomeric IST1 is phosphorylated, and unspecific ULK3 activity is prevented. The next steps towards a better understanding of ULK3 regulation and mechanism of action will likely include the identification of cellular ULK3 interaction partners, structural work on the ULK3 full-length protein and the development of chemical tools for functional studies on the endogenous ULK3 kinase. Our study lays the foundation for this future work.

Acknowledgements

We thank the Kevan Shokat lab (UCSF) for providing the ULK1 and ULK2 expression plasmids. We also thank Roman Fischer and Iolanda Vendrell from the Discovery Proteomics Facility for assistance with the analysis by mass spectrometry. The authors would like to acknowledge funding by the SGC, a registered charity (no: 1097737) that receives funds from AbbVie, Bayer AG, Boehringer Ingelheim, Canada Foundation for Innovation, Eshelman Institute for Innovation, Genentech, Genome Canada through Ontario Genomics Institute [OGI-196], EU/EFPIA/OICR/McGill/KTH/Diamond, Innovative Medicines Initiative 2 Joint Undertaking [EUBOPEN grant 875510], Janssen, Merck KGaA (aka EMD in Canada and US), Merck & Co (aka MSD outside Canada and US), Pfizer, São Paulo Research Foundation-FAPESP, Takeda and Wellcome. S.K. is also grateful for funding by the German translational cancer network (DKTK) the Frankfurt Cancer Centre (FCI) as well as the DFG funded SFB1177 (selective autophagy).

Data Availability Statement

The coordinates and structure factors of the kinase-inhibitor complexes have been deposited to the PDB and are available under <https://www.rcsb.org/structure/6FDY> and <https://www.rcsb.org/structure/6FDZ>, respectively.

References

- [1] Alonso, Y. A. M., Migliano, S. M., and Teis, D. (2016) ESCRT-III and Vps4: a dynamic multipurpose tool for membrane budding and scission, *FEBS J* **283**, 3288-3302.
- [2] Hurley, J. H. (2015) ESCRTs are everywhere, *EMBO J* **34**, 2398-2407.
- [3] McCullough, J., Frost, A., and Sundquist, W. I. (2018) Structures, Functions, and Dynamics of ESCRT-III/Vps4 Membrane Remodeling and Fission Complexes, *Annu Rev Cell Dev Biol* **34**, 85-109.
- [4] Caballe, A., Wenzel, D. M., Agromayor, M., Alam, S. L., Skalicky, J. J., Kloc, M., Carlton, J. G., Labrador, L., Sundquist, W. I., and Martin-Serrano, J. (2015) ULK3 regulates cytokinetic abscission by phosphorylating ESCRT-III proteins, *Elife* **4**, e06547.
- [5] Manning, G., Whyte, D. B., Martinez, R., Hunter, T., and Sudarsanam, S. (2002) The protein kinase complement of the human genome, *Science* **298**, 1912-1934.
- [6] Wong, P. M., Puente, C., Ganley, I. G., and Jiang, X. (2013) The ULK1 complex: sensing nutrient signals for autophagy activation, *Autophagy* **9**, 124-137.
- [7] Kuroyanagi, H., Yan, J., Seki, N., Yamanouchi, Y., Suzuki, Y., Takano, T., Muramatsu, M., and Shirasawa, T. (1998) Human ULK1, a novel serine/threonine kinase related to UNC-51 kinase of *Caenorhabditis elegans*: cDNA cloning, expression, and chromosomal assignment, *Genomics* **51**, 76-85.
- [8] Hurley, J. H., and Young, L. N. (2017) Mechanisms of Autophagy Initiation, *Annu Rev Biochem* **86**, 225-244.
- [9] Degenhardt, K., Mathew, R., Beaudoin, B., Bray, K., Anderson, D., Chen, G., Mukherjee, C., Shi, Y., Gelinas, C., Fan, Y., Nelson, D. A., Jin, S., and White, E. (2006) Autophagy promotes tumor cell survival and restricts necrosis, inflammation, and tumorigenesis, *Cancer Cell* **10**, 51-64.
- [10] Menzies, F. M., Fleming, A., and Rubinsztein, D. C. (2015) Compromised autophagy and neurodegenerative diseases, *Nat Rev Neurosci* **16**, 345-357.
- [11] Braden, C. R., and Neufeld, T. P. (2016) Atg1-independent induction of autophagy by the *Drosophila* Ulk3 homolog, ADUK, *FEBS J* **283**, 3889-3897.
- [12] Young, A. R., Narita, M., Ferreira, M., Kirschner, K., Sadaie, M., Darot, J. F., Tavaré, S., Arakawa, S., Shimizu, S., Watt, F. M., and Narita, M. (2009) Autophagy mediates the mitotic senescence transition, *Genes Dev* **23**, 798-803.
- [13] Maloverjan, A., Piirsoo, M., Kasak, L., Peil, L., Osterlund, T., and Kogerman, P. (2010) Dual function of UNC-51-like kinase 3 (Ulk3) in the Sonic hedgehog signaling pathway, *J Biol Chem* **285**, 30079-30090.
- [14] Han, Y., Wang, B., Cho, Y. S., Zhu, J., Wu, J., Chen, Y., and Jiang, J. (2019) Phosphorylation of Ci/Gli by Fused Family Kinases Promotes Hedgehog Signaling, *Dev Cell* **50**, 610-626 e614.
- [15] Takeuchi, F., Isono, M., Katsuya, T., Yamamoto, K., Yokota, M., Sugiyama, T., Nabika, T., Fujioka, A., Ohnaka, K., Asano, H., Yamori, Y., Yamaguchi, S., Kobayashi, S., Takayanagi, R., Ogihara, T., and Kato, N. (2010) Blood pressure and hypertension are associated with 7 loci in the Japanese population, *Circulation* **121**, 2302-2309.

- [16] Levy, D., Ehret, G. B., Rice, K., Verwoert, G. C., Launer, L. J., Dehghan, A., Glazer, N. L., Morrison, A. C., Johnson, A. D., Aspelund, T., Aulchenko, Y., Lumley, T., Kottgen, A., Vasan, R. S., Rivadeneira, F., Eiriksdottir, G., Guo, X., Arking, D. E., Mitchell, G. F., Mattace-Raso, F. U., Smith, A. V., Taylor, K., Scharpf, R. B., Hwang, S. J., Sijbrands, E. J., Bis, J., Harris, T. B., Ganesh, S. K., O'Donnell, C. J., Hofman, A., Rotter, J. I., Coresh, J., Benjamin, E. J., Uitterlinden, A. G., Heiss, G., Fox, C. S., Witteman, J. C., Boerwinkle, E., Wang, T. J., Gudnason, V., Larson, M. G., Chakravarti, A., Psaty, B. M., and van Duijn, C. M. (2009) Genome-wide association study of blood pressure and hypertension, *Nat Genet* **41**, 677-687.
- [17] Luciano, M., Huffman, J. E., Arias-Vasquez, A., Vinkhuyzen, A. A., Middeldorp, C. M., Giegling, I., Payton, A., Davies, G., Zgaga, L., Janzing, J., Ke, X., Galesloot, T., Hartmann, A. M., Ollier, W., Tenesa, A., Hayward, C., Verhagen, M., Montgomery, G. W., Hottenga, J. J., Konte, B., Starr, J. M., Vitart, V., Vos, P. E., Madden, P. A., Willemsen, G., Konnerth, H., Horan, M. A., Porteous, D. J., Campbell, H., Vermeulen, S. H., Heath, A. C., Wright, A., Polasek, O., Kovacevic, S. B., Hastie, N. D., Franke, B., Boomsma, D. I., Martin, N. G., Rujescu, D., Wilson, J. F., Buitelaar, J., Pendleton, N., Rudan, I., and Deary, I. J. (2012) Genome-wide association uncovers shared genetic effects among personality traits and mood states, *Am J Med Genet B Neuropsychiatr Genet* **159B**, 684-695.
- [18] Chaikuad, A., Koschade, S. E., Stolz, A., Zivkovic, K., Pohl, C., Shaid, S., Ren, H., Lambert, L. J., Cosford, N. D. P., Brandts, C. H., and Knapp, S. (2019) Conservation of structure, function and inhibitor binding in UNC-51-like kinase 1 and 2 (ULK1/2), *Biochem J* **476**, 875-887.
- [19] Lazarus, M. B., Novotny, C. J., and Shokat, K. M. (2015) Structure of the human autophagy initiating kinase ULK1 in complex with potent inhibitors, *ACS Chem Biol* **10**, 257-261.
- [20] Lazarus, M. B., and Shokat, K. M. (2015) Discovery and structure of a new inhibitor scaffold of the autophagy initiating kinase ULK1, *Bioorg Med Chem* **23**, 5483-5488.
- [21] Nicolaou, C. A., Humblet, C., Hu, H., Martin, E. M., Dorsey, F. C., Castle, T. M., Burton, K. I., Hu, H., Hendle, J., Hickey, M. J., Duerksen, J., Wang, J., and Erickson, J. A. (2019) Idea2Data: Toward a New Paradigm for Drug Discovery, *ACS Med Chem Lett* **10**, 278-286.
- [22] Preuss, F., Chatterjee, D., Mathea, S., Shrestha, S., St-Germain, J., Saha, M., Kannan, N., Raught, B., Rottapel, R., and Knapp, S. (2020) Nucleotide Binding, Evolutionary Insights, and Interaction Partners of the Pseudokinase Unc-51-like Kinase 4, *Structure*.
- [23] Khamrui, S., Ung, P. M. U., Secor, C., Schlessinger, A., and Lazarus, M. B. (2020) High-Resolution Structure and Inhibition of the Schizophrenia-Linked Pseudokinase ULK4, *J Am Chem Soc* **142**, 33-37.
- [24] Blagg, J., and Workman, P. (2017) Choose and Use Your Chemical Probe Wisely to Explore Cancer Biology, *Cancer Cell* **32**, 9-25.
- [25] Drewes, G., and Knapp, S. (2018) Chemoproteomics and Chemical Probes for Target Discovery, *Trends Biotechnol.*
- [26] Burgess-Brown, N. A., Mahajan, P., Strain-Damerell, C., Gileadi, O., and Graslund, S. (2014) Medium-throughput production of recombinant human proteins: protein production in *E. coli*, *Methods Mol Biol* **1091**, 73-94.
- [27] Niesen, F. H., Berglund, H., and Vedadi, M. (2007) The use of differential scanning fluorimetry to detect ligand interactions that promote protein stability, *Nat Protoc* **2**, 2212-2221.
- [28] Winter, G. (2010) xia2: an expert system for macromolecular crystallography data reduction, *Journal of Applied Crystallography* **43**, 186-190.
- [29] McCoy, A. J., Grosse-Kunstleve, R. W., Storoni, L. C., and Read, R. J. (2005) Likelihood-enhanced fast translation functions, *Acta Crystallogr D Biol Crystallogr* **61**, 458-464.
- [30] Murshudov, G. N., Vagin, A. A., and Dodson, E. J. (1997) Refinement of macromolecular structures by the maximum-likelihood method, *Acta Crystallogr D Biol Crystallogr* **53**, 240-255.
- [31] Chen, V. B., Arendall, W. B., 3rd, Headd, J. J., Keedy, D. A., Immormino, R. M., Kapral, G. J., Murray, L. W., Richardson, J. S., and Richardson, D. C. (2010) MolProbity: all-atom structure validation for macromolecular crystallography, *Acta Crystallogr D Biol Crystallogr* **66**, 12-21.
- [32] Mathea, S., Abdul Azeez, K. R., Salah, E., Tallant, C., Wolfreys, F., Konietzny, R., Fischer, R., Lou, H. J., Brennan, P. E., Schnapp, G., Pautsch, A., Kessler, B. M., Turk, B. E., and Knapp, S. (2016) Structure of the Human Protein Kinase ZAK in Complex with Vemurafenib, *ACS Chem Biol* **11**, 1595-1602.

- [33] Buchan, D. W. A., and Jones, D. T. (2019) The PSIPRED Protein Analysis Workbench: 20 years on, *Nucleic Acids Res* 47, W402-W407.
- [34] Taylor, S. S., and Kornev, A. P. (2011) Protein kinases: evolution of dynamic regulatory proteins, *Trends Biochem Sci* 36, 65-77.
- [35] Adams, J. A. (2003) Activation loop phosphorylation and catalysis in protein kinases: is there functional evidence for the autoinhibitor model?, *Biochemistry* 42, 601-607.
- [36] Fedorov, O., Niesen, F. H., and Knapp, S. (2012) Kinase inhibitor selectivity profiling using differential scanning fluorimetry, *Methods Mol Biol* 795, 109-118.
- [37] Ren, H., Bakas, N. A., Vamos, M., Chaikuad, A., Limpert, A. S., Wimer, C. D., Brun, S. N., Lambert, L. J., Tautz, L., Celeridad, M., Sheffler, D. J., Knapp, S., Shaw, R. J., and Cosford, N. D. P. (2020) Design, Synthesis, and Characterization of an Orally Active Dual-Specific ULK1/2 Autophagy Inhibitor that Synergizes with the PARP Inhibitor Olaparib for the Treatment of Triple-Negative Breast Cancer, *J Med Chem* 63, 14609-14625.
- [38] Zhao, G., Li, W. Y., Chen, D., Henry, J. R., Li, H. Y., Chen, Z., Zia-Ebrahimi, M., Bloem, L., Zhai, Y., Huss, K., Peng, S. B., and McCann, D. J. (2011) A novel, selective inhibitor of fibroblast growth factor receptors that shows a potent broad spectrum of antitumor activity in several tumor xenograft models, *Mol Cancer Ther* 10, 2200-2210.
- [39] Piirsoo, A., Kasak, L., Kauts, M. L., Loog, M., Tints, K., Uusen, P., Neuman, T., and Piirsoo, M. (2014) Protein kinase inhibitor SU6668 attenuates positive regulation of Gli proteins in cancer and multipotent progenitor cells, *Biochim Biophys Acta* 1843, 703-714.
- [40] Levinson, N. M., and Boxer, S. G. (2012) Structural and spectroscopic analysis of the kinase inhibitor bosutinib and an isomer of bosutinib binding to the Abl tyrosine kinase domain, *PLoS One* 7, e29828.
- [41] Forsyth, T., Kearney, P. C., Kim, B. G., Johnson, H. W., Aay, N., Arcalas, A., Brown, D. S., Chan, V., Chen, J., Du, H., Epshteyn, S., Galan, A. A., Huynh, T. P., Ibrahim, M. A., Kane, B., Koltun, E. S., Mann, G., Meyr, L. E., Lee, M. S., Lewis, G. L., Noguchi, R. T., Pack, M., Ridgway, B. H., Shi, X., Takeuchi, C. S., Zu, P., Leahy, J. W., Nuss, J. M., Aoyama, R., Engst, S., Gendreau, S. B., Kassees, R., Li, J., Lin, S. H., Martini, J. F., Stout, T., Tong, P., Woolfrey, J., Zhang, W., and Yu, P. (2012) SAR and in vivo evaluation of 4-aryl-2-aminoalkylpyrimidines as potent and selective Janus kinase 2 (JAK2) inhibitors, *Bioorg Med Chem Lett* 22, 7653-7658.
- [42] Adams, P. D., Afonine, P. V., Bunkoczi, G., Chen, V. B., Davis, I. W., Echols, N., Headd, J. J., Hung, L. W., Kapral, G. J., Grosse-Kunstleve, R. W., McCoy, A. J., Moriarty, N. W., Oeffner, R., Read, R. J., Richardson, D. C., Richardson, J. S., Terwilliger, T. C., and Zwart, P. H. (2010) PHENIX: a comprehensive Python-based system for macromolecular structure solution, *Acta Crystallogr D Biol Crystallogr* 66, 213-221.
- [43] Huse, M., and Kuriyan, J. (2002) The conformational plasticity of protein kinases, *Cell* 109, 275-282.
- [44] Sultan, M. M., Denny, R. A., Unwalla, R., Lovering, F., and Pande, V. S. (2017) Millisecond dynamics of BTK reveal kinome-wide conformational plasticity within the apo kinase domain, *Sci Rep* 7, 15604.
- [45] Lakkaniga, N. R., Balasubramaniam, M., Zhang, S., Frett, B., and Li, H. Y. (2019) Structural Characterization of the Aurora Kinase B "DFG-flip" Using Metadynamics, *AAPS J* 22, 14.
- [46] Pinto-Fernandez, A., Davis, S., Schofield, A. B., Scott, H. C., Zhang, P., Salah, E., Mathea, S., Charles, P. D., Damianou, A., Bond, G., Fischer, R., and Kessler, B. M. (2019) Comprehensive Landscape of Active Deubiquitinating Enzymes Profiled by Advanced Chemoproteomics, *Front Chem* 7, 592.

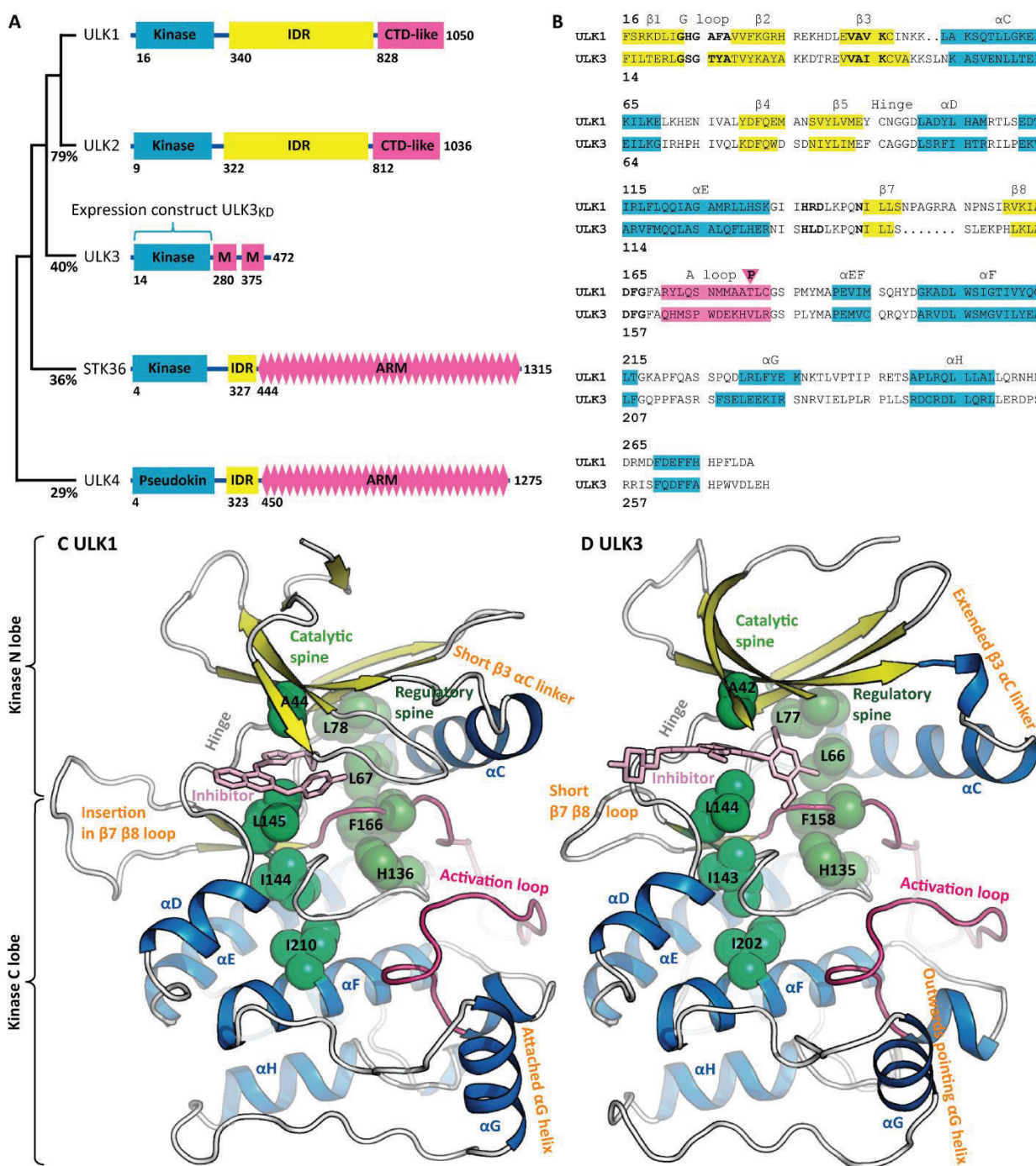


Figure 1A) The ULK family of protein kinases has derived from subsequent gene duplications. All five family members contain the kinase domain in their N terminus and long C-terminal extensions. CTD-like – carboxy terminal domain-like domain; M – microtubule interacting and trafficking molecule (MIT) domain; ARM – armadillo repeat domain; IDR – intrinsically disordered region. The percentages describe the identities with the ULK1 kinase domain sequence. The blue brackets indicate the ULK3 expression construct used in this study. **B)** Alignment of ULK1 and ULK3 kinase domain sequences. β strands are highlighted in yellow, α helices in blue, the activation loops in pink, and conserved kinase motifs are in bold. Please note the unusual insertions between the $\beta 7$ and $\beta 8$ strands and the sequence variability in the activation loops / the αG helices. **C and D)** Comparison of the ULK1 (PDB ID 5C17) and ULK3 kinase domains (PDB ID 6FDY). Regions with obvious differences are labelled in orange. Both kinases adopt the active-like conformation with fully assembled hydrophobic spines.

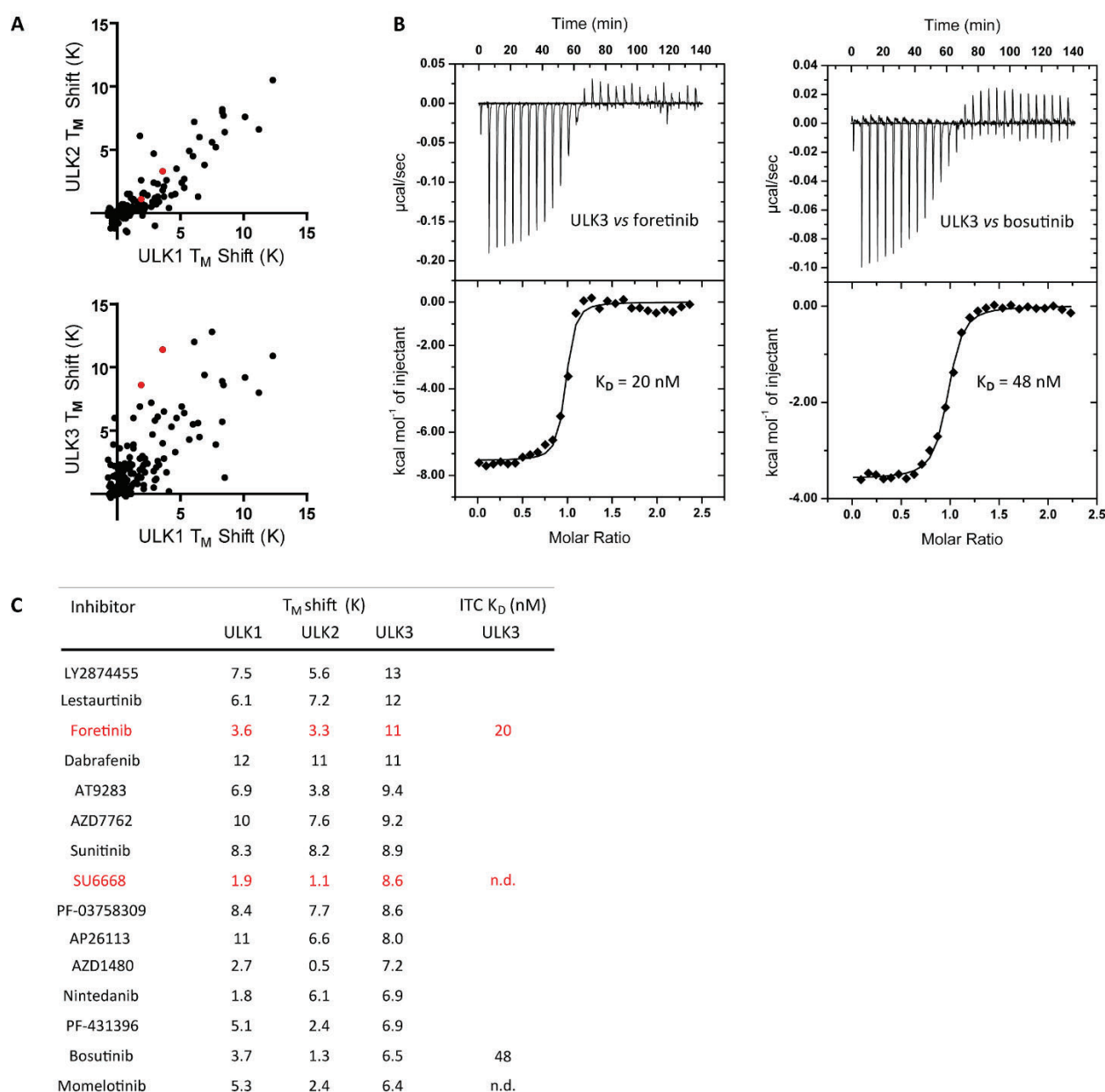
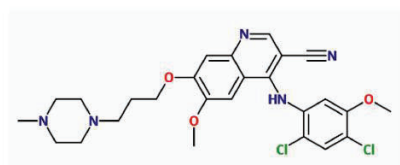


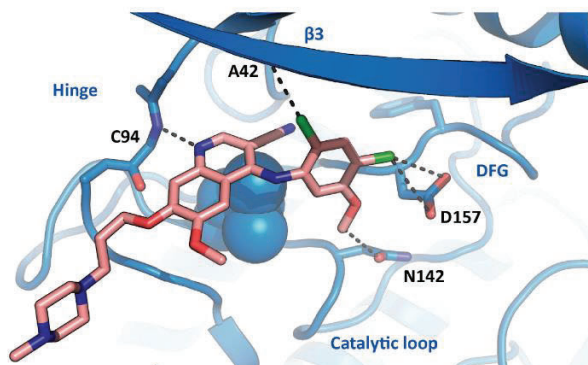
Figure 2A) 150 clinical kinase inhibitors were tested for their ability to stabilise ULK1, ULK2 or ULK3 in differential scanning fluorimetry (DSF). Several of the inhibitors induced melting temperature (T_M) shifts. The cross-correlation plots reveal that ULK1 and ULK2 were targeted by a similar subset of inhibitors, while the inhibitors stabilizing ULK1 and ULK3 differed. **B)** The binding of some of the DSF hits to ULK3 was validated by isothermal titration calorimetry (ITC). Foretinib and bosutinib bound ULK3 with K_D values of 20 and 48 nM, respectively. **C)** Summary of DSF and ITC assay results for the best ULK3 binders. Foretinib and SU6668 showed some selectivity for ULK3 over ULK1/2.

A Bosutinib

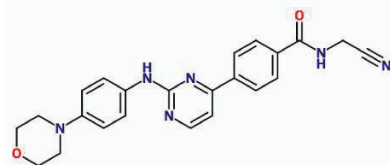


T_M shift = 6.5 K

ITC K_D = 48 nM



B Momelotinib



T_M shift = 6.4 K

ITC K_D n.d.

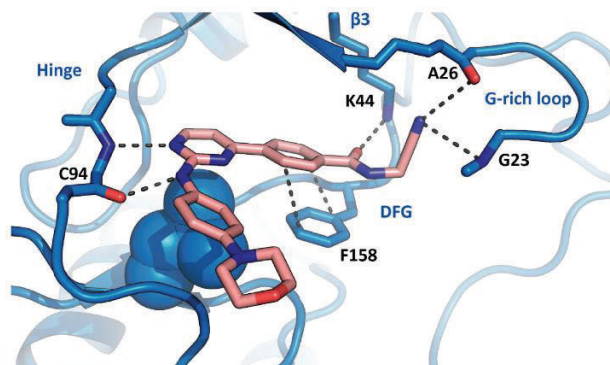


Figure 3A) Binding mode of bosutinib to the ULK3 active site. The quinoline nitrogen anchored the inhibitor to C94 in the hinge. The substituents of the terminal 6-ring formed hydrogen bonds to the A42 backbone oxygen in the $\beta 3$ strand, to D157 in the DFG motif, and to the conserved N142 prior to the $\beta 7$ strand (PDB ID 6FDY). **B)** Momelotinib was anchored to C94 in the ULK3 hinge, too, but the other inhibitor interactions with ULK3 were different from what was observed for bosutinib. Its nitrile pointed towards the ULK3 glycine-rich loop, forming interactions with G23 and A26 backbone atoms. One of the biphenyl rings recruited the DFG F158 sidechain for a π -stacking interaction, thus stabilising ULK3 in the DFG-out conformation. And finally, the momelotinib amide oxygen tightly bound the conserved K44 in the $\beta 3$ strand (PDB ID 6FDZ). For clarity, parts of the $\beta 1$ and $\beta 2$ strands were removed from the models.

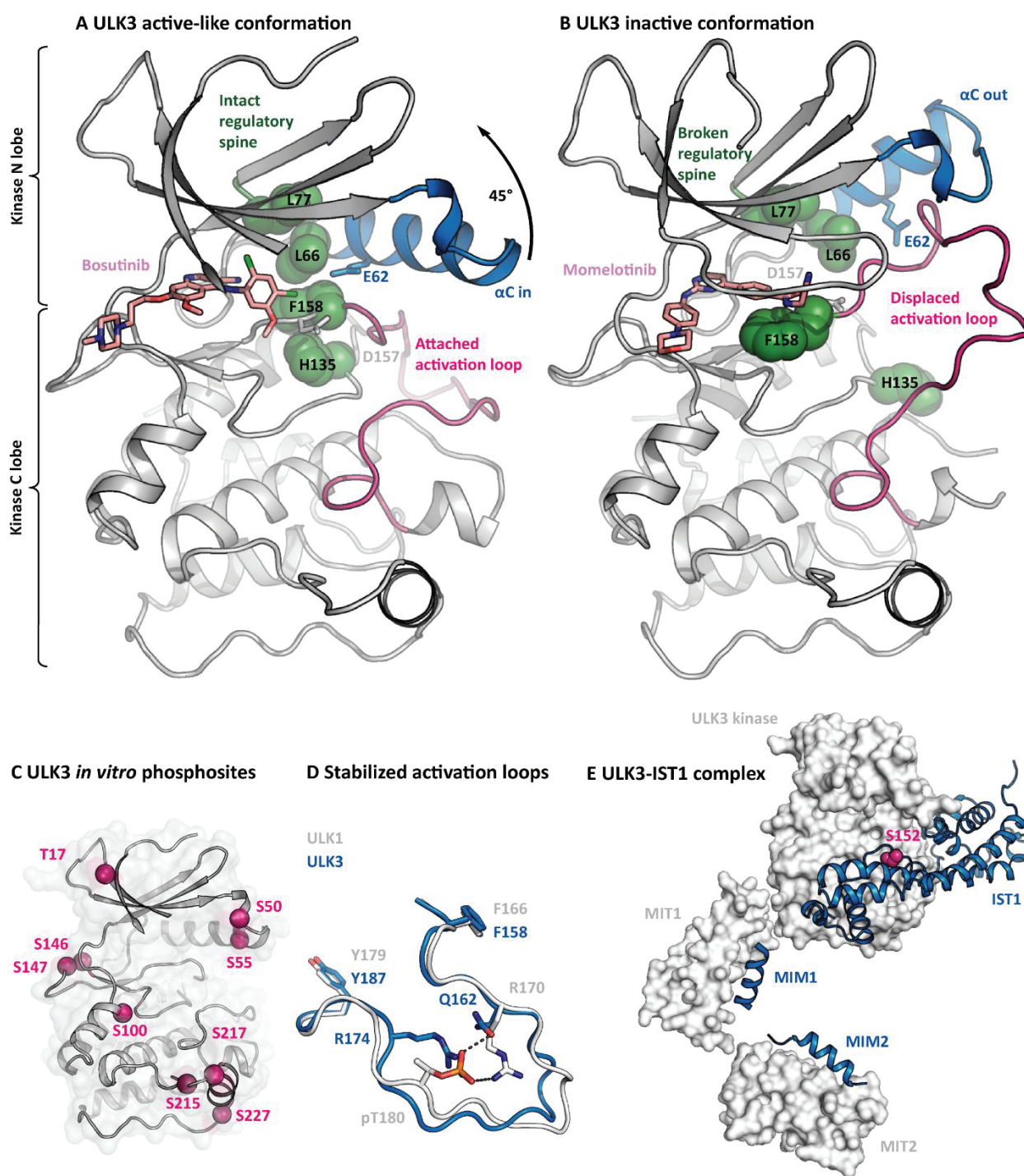


Figure 4 **A)** Domain plasticity of the ULK3 kinase. In the active-like conformation, the regulatory spine was fully assembled, and the activation loop attached (PDB ID 6FDY). **B)** In the inactive conformation, the regulatory spine was broken, and the activation loop displaced (PDB ID 6FDZ). **C)** The recombinant ULK3 kinase domain was constitutively active and readily autophosphorylated. The phosphosites (indicated in pink) were embedded in flexible loop regions. Please note that the activation loop was spared from autophosphorylation. **D)** Despite their differing sequences, the ULK1 and ULK3 activation loops adopted very similar conformations. They were closely attached to the C lobe, allowing for substrate docking. In ULK1, this conformation was stabilized by T180 phosphorylation. In ULK3, no phosphorylation was necessary for the formation of the Q162 to R174 salt bridge, promoting a constitutively active conformation. **E)** Model of the ULK3-IST1 complex. The IST1 MIM helices bind to the ULK3 MIT tandem, the IST1 polymerization domain binds to the ULK3 kinase domain. The phosphoacceptor S152 is proximal to the kinase active site. Modelling done with phenix.dynamics.⁴² PDB IDs ULK3 6FDY, IST1 3FRR, MIT1/MIM1 4U7Y, MIT2/MIM2 4WZX.

MGSHHHHHHS SGTENLYFQA GPGWGPPRLD GFILTERLGS GTYATVYKAY AKKDTREVVA
 IKCVAKKSLN KASVENLLTE IEILKGIRHP HIVQLKDFQW DSDNIYLIME FCAGGDLRF
 IHTRRILPEK VARVFMQQLA SALQFLHERN ISHLDLKPQN ILLSSLEKPH LKLADFGFAQ
 HMPSPWDEKLV LRGSPYMAP EMVCQRQYDA RVDLWSMGVI LYEALFGQPP FASRSFSELE
 EKIRSNRVIE LPLRPILLSRD CRDLLQRLLE RDPSRRISFQ DFFAHPWVDL EHMP

Figure S1) Sequence of the expression construct His₆-TEV-ULK3₂₋₂₇₇.

Table S1. X-Ray Crystallography Data Collection and Refinement Statistics

	ULK3-bosutinib	ULK3-momelotinib
PDB ID	6FDY	6FDZ
Space group	C 2 2 2	P 6 ₁ 2 2
Cell parameters		
a, b, c (Å)	92.38, 169.40, 45.92	75.84, 75.84, 214.69
α, β, γ (°)	90, 90, 90	90, 90, 120
Resolution (Å)	48.18 - 1.70 (1.73 - 1.70)*	65.68 - 2.55 (2.59 - 2.55)*
Unique reflexions	39968 (3929)*	12747 (1230)*
Completeness for range (%)	100 (99.1)*	100 (100)*
Multiplicity	6.5 (6.0)*	18.7 (19.7)*
R_{merge}	0.09 (0.824)*	0.14 (1.636)*
I/σ(I)	13.4 (2.1)*	17.0 (2.2)*
Wavelength (Å)	0.9282	0.9686
Phasing	MR	MR
R_{work}, R_{free} (%)	20.5, 23.9	23.1, 28.5
Number of atoms		
protein, other, solvent	2048, 72, 127	2029, 31, 7
B-factors (Å²)		
protein, other, solvent	25.2, 27.1, 27.9	62.7, 54.6, 51.5
rmsd bond (Å)	0.022	0.013
rmsd angle (°)	1.91	1.69
Ramachandran statistics		
favoured, outliers (%)	96.51, 0.39	91.95, 1.15

*Values in parentheses correspond to the highest resolution shell.

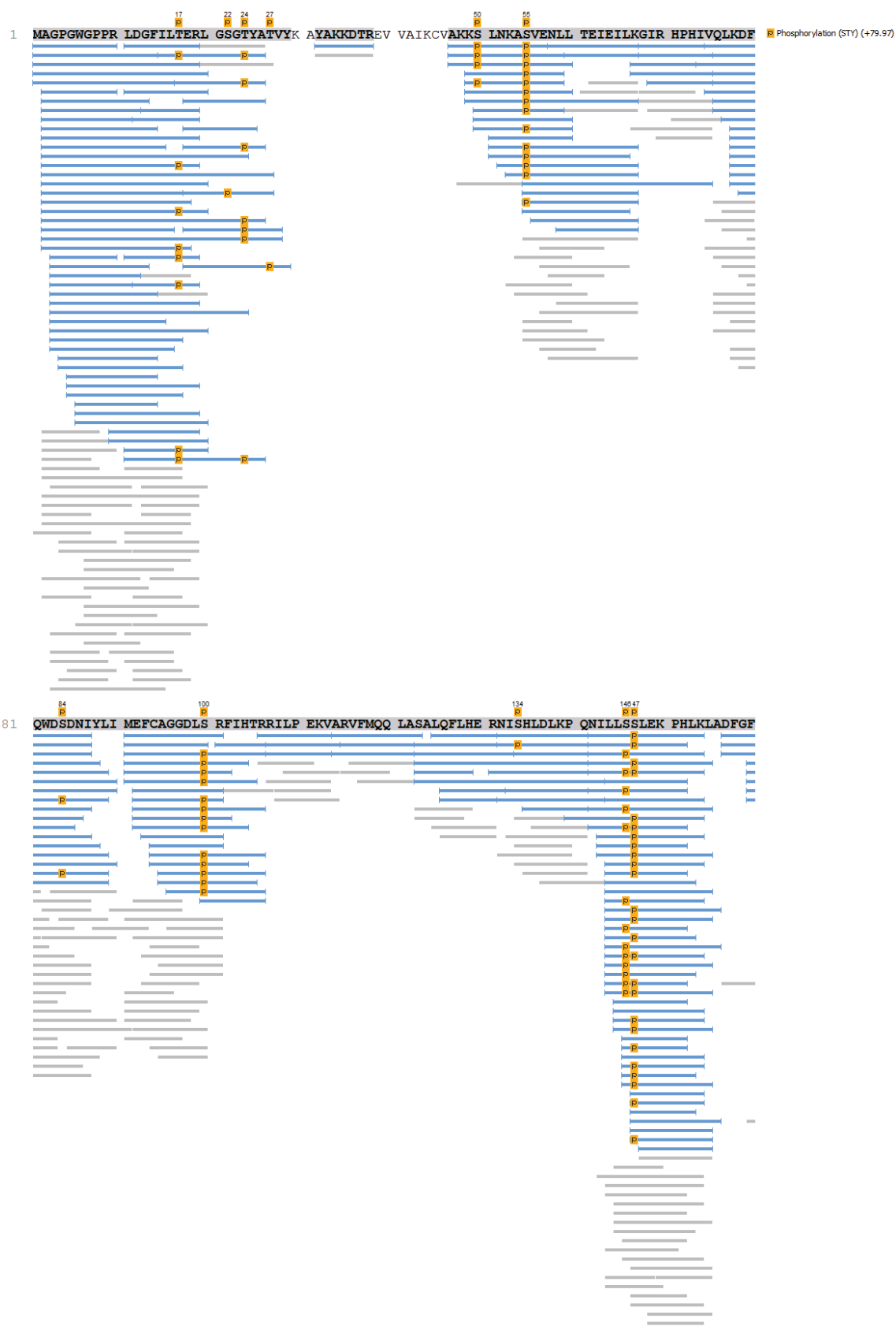




Figure S2) ULK3 phosphosite mapping by mass spectrometry. The autophosphorylated ULK3 kinase domain was digested with elastase and analysed by LC-MS/MS. The mass spectrometry dataset was evaluated using the software PEAKS (v8, Bioinformatics Solutions Inc) as described previously.⁴⁶ Peptides identified with high confidence are shown in blue, and phosphorylated S/T/Y residues are highlighted in orange. Notably, no extensive phosphorylation was detected in the ULK3 activation segment (residues D157 to E183). In contrast, several serine residues situated in flexible loop regions such as S55 in the $\beta 3$ αC linker, S146 in the $\beta 7$ $\beta 8$ insert, and S215 in the αF αG loop, were highly phosphorylated, reflected by the number of detected phosphopeptides.

Table S2. Impact of 150 small molecules on the ULK1, ULK2 and ULK3 thermostability (DSF assay)

Compound	ULK1 T _M Shift (K)	ULK2 T _M Shift (K)	ULK3 T _M Shift (K)	SMILES
Vandetanib	0.1	0.3	0.0	CN1CCC(CC1)COC2=C(C=C3C(=C2)N=CN=C3NC4=C(C=C(C=C4)Br)F)OC
PF-04691502	0.5	0.7	0.0	O=C1N([C@H]2CC[C@H](OCCO)CC2)C3=NC(N)=NC(C)=C3C=C1C4=CN=C(OC)C=C4
Tivozanib	0.1	0.1	0.6	O=C(Nc1noc(c1)Nc4cccc(OC2c3cc1OC)c(OC)cc3ccc2)cc4Cl
Ruxolitinib	3.2	2.3	2.6	c1c[nH]c2c1c(ncn2)c3cnnc(c3)[C@H](C#N)C4CCCC4
Refametinib	1.7	0.3	1.4	FC1=CC(OC)=C(NS(C2(CC2)C[C@H](O)CO)=(O)=O)C(NC3=CC=C(I)C=C3F)=C1F
Linsitinib	0.3	0.5	0.4	C[C@]1(C[C@H])(C1)C2=NC(=C3N2C=CN=C3N)C4=CC5=C(C=CC(=N5)C6=CC=CC=C6)C=C4)O
OSI-027	0.8	0.6	2.2	COC1=CC=CC2=CC(=C3C4=C(C=N=C3)C=CN4C(=N3)C5CCC(C5)C(=O)O)N=N=C1
EMD1214063	-0.3	0.1	0.4	CN1CCC(CC1)COC2=CN=C(N=C2)C3=CC(=CC=C3)CN4C(=O)C=CC(=N4)C5=CC=CC(=C5)C#N
Alisertib	-0.3	-0.1	3.9	COC1=C(C(=C=C1)F)C2=NC3C=CN=C(N=C3C4=C2C=C(C=C4)C)N(C5=CC(=C(C=C5)C(=O)O)OC
AZD8055	-0.6	0.0	-0.1	CC1COCCN1C2=NC(=NC3=C2NC(=C3)C4=C(C=C(C=C4)OC)CO)N5CCOCC5C
BMS-754807	3.9	2.6	1.7	FC1=NC=C(NC([C@]2(C)CCCN2C3=NN4C(C(NC5=NNC(C6CC6)=C5)=N3)=CC=C4)=O)C=C1
Idelalisib	-0.5	0.3	-0.3	Fe2cccc3N=C/N(C1cccc1C)(C=O)c23)[C@@H](Nc4nnc5nncn45)CC
Motesanib	0.6	0.5	0.3	O=C(c2ccnc2Nc1c1cncc1)Nc3ccc4c(c3)NCC4(C)C
Palbociclib	2.9	4.7	0.5	O=C2N(c1nc(ncc1)/C(=C2)/C(=O)C)Nc3ccc(cc3)N4CCNCC4)C5CCCC5
Selumetinib	0.1	0.1	1.9	CN1C=NC2=C1C=C(C(=C2F)NC3=C(C(=C(C=C3)Br)Cl)C(=O)NOCCO
SNS-032	0.8	-1.5	1.1	CC(C)(C)c1oc(CSc2cnc(NC(=O)C3CCNCC3)s2)nc1
Afatinib	0.0	-0.4	1.3	CN(C)C\C=C\C(=O)Nc3cc1c(Nc(c2C1)ccc2F)ncnc1cc3OC4COCC4
Alvocidib	0.5	0.5	0.9	Clc4cccc4C=2Oc1c(c(O)cc(O)c1C(=O)=C2)[C@H]3CCN(C)[C@H]3O
Axitinib	6.5	6.0	4.5	O=C(NC)c4cccc4Sc1ccc2c(c1)nnc2\C=C\c3ncccc3
Water	0.1	-0.8	0.4	O
Enzastaurin	1.9	2.6	1.3	O=C3C(\c2c1cccc1n(c2)C)=C(/C(=O)N3)c5c4cccc4n(c5)C7CCN(C6bncccc6)CC7
Pictilisib	-0.3	-0.8	1.4	CS(N(CC1)CCN1CC(S2)=CC3=C2C(N4CCOCC4)=NC(C5=C(C=NN6)C6=CC=C5)=N3)(=O)=O
Nilotinib	0.7	-0.4	0.3	Cc1ccc(cc1Nc2nccc(n2)c3ccnc3C)C(=O)Nc4cc(cc(c4)n5ccc(nc5)C)C(F)(F)F
Saracatinib	2.1	1.6	2.3	CN1CCN(C1)CCOC2=CC3=C(C(=C2)OC4CCOCC4)=N(N=N3)NC5=C(C(=CC6=C5OCO6)Cl
Midostaurin	-0.2	-0.3	6.0	C[C@]12[C@H](C[C@H])(C[C@H])(O1)N314CC=CC=C4C5=C6C(C=C8N27C53)CNC6=O)N(C)[C(=O)C9=CC=CC=C9)OC
AZ3146	1.6	0.9	1.2	CN1CCC(CC1)OC2=CC(=C(C(=C2)NC3=NC=C4C(=N3)N(C(=O)N4C)C5CCCC5)OC
Cediranib	0.6	-0.1	2.0	Cc4nc5ccc(Oc3nnc2cc(OCCCN1CCCC1)c(OC)cc23)c(F)c5c4
Sunitinib	8.3	8.2	8.9	CCN(C)CCNCC(=O)c1c(c([nH]c1)/C=C\2/c3ccc(ccc3NC2=O)F)C
AZD1152-HQPA	0.5	0.5	1.8	CCN(CCCOC1=CC2=C(C=C1)C(=NC=N2)NC3=NNC(=C3)CC(=O)NC4=CC(=CC=C4)F)CCO
MK-2206	-0.4	-0.6	0.3	C1CC(C1)(C2=CC=C(C(=C2)C3=C(C(=C4C(=N3)C=CN5C4=NNC5=O)C6=CC=CC=C6)N
AZD7762	10.1	7.6	9.2	O=C(N[C@H]1CNCCC1)C2=C(NC(N)=O)C=C(C3=CC=CC(F)C3)S2
Trametinib	-0.4	-0.8	0.3	Ic1ccc(c(F)c1N)\C3=C\2/C(=O)N(C(=O)N(C/2=C(\C(=O)N3C)C)c4cccc(NC(=O)C)c4)C5CC5
BI 2536	0.6	-0.1	1.3	CCC1C(=O)N(C2=CN=C(N=C2N1C3CCCC3)NC4=C(C(=C(C=C4)C(=O)N5CCN(CC5)C)OC)C
Foretinib	3.6	3.3	11.4	COC1=CC2=C(C=CN=C2C=1C1OCCCN3CCOC3)OC4=C(C(=C(C=C4)NC(C(=O)N6=CC=C(C=C6)F)F
Ponatinib	6.0	4.5	5.5	Cc1ccc(cc1C#Cc2cnc3n2nccc3)C(=O)Nc4ccc(c(c4)C(F)(F)F)CN5CCN(CC5)C
Lestaurtinib	6.1	7.2	12.0	C[C@]12[C@]([C[C@H])(O1)n3c4cccc4c5c3c6n2c7cccc7c6c85C(=O)NC8)(CO)O
Imatinib	0.6	0.1	-0.1	Cc1ccc(cc1Nc2nccc(n2)c3ccnc3)NC(=O)c4ccc(cc4)CN5CCN(CC5)C
Lapatinib	0.7	-1.4	0.9	CS(=O)=O)CCNCc1ccc(o1)c2ccc3c(c2)c(ncn3)Nc4ccc(c(c4)Cl)OC5cccc(c5)F
Nintedanib	1.8	6.1	6.9	CN1CCN(CC1)CC(=O)N(C)C2=CC=C(C(=C2)N/C(=C\3/4=C(C(=C(C4)C(=O)OC)NC3=O)/C5=CC=CC=C5
Buparlisib	0.7	-0.3	0.5	NC(N=C1)=CC(C(F)(F)F)=C1C2=CC(N3CCOCC3)=NC(N4CCOCC4)=N2
Linifanib	3.7	2.1	2.8	CC1=CC(=C(C(=C1)F)NC(=O)NC2=CC=C(C(=C2)C3=C4C(=CC=C3)NN=C4N
Galunisertib	-0.2	-0.3	0.5	NC(C1=CC(C(C2=C(CCC3)N3N=C2C4=NC(C)=CC=C4)=CC=N5)=C5C=C1)=O
Rabusertib	0.3	-0.1	1.7	Cc1cc(c(cc1Br)NC(=O)Nc2cnc(cn2)C)OC[C@H]3CNCCO3
RAF265	2.0	-0.2	3.0	CN1C2=C(C(=C(C(=C2)OC3=CC(=NC=C3)C4=NC=C(N4)C(F)(F)F)N=C1NC5=CC=C(C(=C5)C(F)(F)F
Brivanib	-0.2	-1.2	2.2	CC1=CC2=C(C1)C=CC(=C2F)OC3=CC=C(NC4C3=C(C(=C4)OC)C(C(=O)N)C(C)OC
PF-04708671	0.4	-0.3	0.8	CCC1=CN=CN=C1N(CC2)CCN2CC3=NC4=CC(C(F)(F)F)=CC=C4N3[H]
Tamatinib	8.5	6.4	1.3	COc1cc(Nc2ncc(c(n2)Nc2ccc3(n2)N(COP(=O)([O-])[O-])C(=O)C(O3)(C

Doramapimod	0.3	0.0	0.5	CC1=CC=C(C=C1)N2C(=CC(=N2)C(C)(C)C)NC(=O)NC3=CC=C(C4=CC=CC=C43)OCCN5CCOCC5
Pilaralisib	0.2	0.1	0.5	CC(C)(C(=O)NC1=CC(=CC=C1)S(=O)(=O)NC2=NC3=CC=CC=C3N=C2NC4=C(C(=CC(=C4)OC)C)I)N
Pimasertib	-0.4	0.0	0.1	C1=CC(=C(C=C1)F)NC2=C(C(=CN=C2)C(=O)NCC(CO)O
AT9283	6.9	3.8	9.4	c1cc2c(cc1CN3CCOCC3)nc([nH]2)c4c(c[nH]n4)NC(=O)NC5CC5
Crizotinib	3.1	0.7	1.2	C[C@H](C1=C(C=CC(=C1Cl)F)Cl)OC2=C(N=CC(=C2)C3=CN(N=C3)C4CCNCC4)N
CUDC-101	0.3	0.2	0.1	COC1=C(C=C2C(=C1)N=CN=C2NC3=CC=CC(=C3)C#C)OCCCCC(C(=O)NO
Danuseritib	1.2	0.5	0.7	CN1CCN(CC1)C2=C=C(C(=C2)C(=O)NC3=NNC4=C3CN(C4)C(=O)C(C5=CC=CC=C5)OC
Dovitinib	0.7	0.2	0.0	CC(C(=O)O)O.CC(C(=O)O)O.CN1CCN(CC1)C2=CC3=C(C(=N2)NC(=C4C(=C5C(=NC4=O)C=CC=C5F)N)N3
MGCD-265	0.7	0.2	-0.1	CN1C=C(N=C1)C2=CC3=NC=CC(=C3S2)OC4=C(C(=C=C4)NC(=S)NC(=O)CC5=CC=CC=C5)F
Fasudil	2.1	0.5	0.7	C1CNCCN(C1)S(=O)(=O)C2=CC=CC3=C2C=CN=C3
Masitinib	-0.6	-0.2	0.0	O=C(c1cccc(cc1)CN2CCN(C)CC2)Nc3cc(c(cc3)C)Nc4nc(cs4)c5ccccc5
Pazopanib	-2.1	-0.4	2.9	CC1=C(C=C(C=C1)NC2=NC=CC(=N2)N(C)C3=CC4=NN(C(=C4C=C3)C)C)S(=O)(=O)N
Seliciclib	-0.5	-0.2	0.8	CC[C@H](CO)NC1=NC(=C2C(=N1)N(C(=N2)C(C)C)NCC3=CC=CC=C3
Vatalanib	0.3	0.0	1.4	C1c1ccc(cc1)Nc3nnc(c2c3cccc2)Cc4cncc4
Tofacitinib	-0.1	-0.3	1.5	CC1CCN(CCN1N(C)C2=NC=NC3=C2C=CN3)C(=O)CC#N
Dactolisib	-0.3	-0.4	0.5	N#CC(c6ccc(N5c4c(cnc3ccc(c1cc2cccc2nc1)cc34)N(C5=O)C)cc6)(C)C
Gandotinib	2.8	0.9	4.7	CC1=NNC(NC2=NN3C(C(CN4CCOCC4)=C2)=NC(C)=C3CC5=CC=C(C)C(=C5F)=C1
Regorafenib	1.8	0.7	1.9	CNC(=O)C1cc(ccn1)Oc2ccc(c(c2)F)NC(=O)Nc3ccc(c(c3)C(F)F)Cl.O
Ruboxistaurin	1.3	0.4	1.6	CN(C)CC1CN2C=C(C3=CC=CC=C32)C4=C(C5=CN(CCO1)C6=CC=CC=C65)C(=O)NC4=O
Sotrastaurin	1.1	1.2	0.5	CN1CCN(CCN1)C2=NC3=CC=CC=C3C(=N2)C4=C(C(=O)NC4=O)C5=CNc6=CC=CC=C65
Voxtalisisb	1.1	0.4	0.1	COC1=CC(NC2=NC=CC=C3N=C2NS(C4=CC=C(NC(C5=CC(C)OC(=C(C)C5=O)C(=C4)O)=O)C(=C)OC(=O)=C1
Tandutinib	-0.2	0.1	-0.1	CC(C)OC1=CC=C(C=C1)NC(=O)N2CCN(CCN2)C3=NC=NC4=CC(=C(C=C43)OC)OCCCN5CCCCC5
Sorafenib	3.0	-1.0	1.1	CNC(=O)C1cc(ccn1)Oc2ccc(cc2)NC(=O)Nc3ccc(c(c3)C(F)F)F)Cl
Quizartinib	-0.7	-0.2	1.3	CC(C)(C)c1cc(no1)NC(=O)Nc2ccc(cc2)c3cn4c5ccc(cc5sc4n3)OCCN6CCOCC6
Solisolisb	0.2	-0.2	1.6	CC(=O)OC1C(CCC2=O)C3=C1C4(OC(=O)C(C(=CN(CC=C4)C)C)C)C4=C(C3=O)O)COC(C)C
Apitolisib	0.2	-0.2	3.6	Cc1c(sc2c1nc(nc2N3CCOCC3)c4nc(nc4)N)CN5CCN(CCN5)C(=O)[C@H](C)O
Tivantinib	0.3	0.0	1.9	C1CC2=C3C(=CC=C2)C(=CN3C1)[C@H]4[C@@H](C(=O)NC4=O)C5=CNc6=CC=CC=C65
MEK-162	-0.5	-0.2	2.3	CN1C=NC2=C1C(=C(C2F)NC3=C(C(=C3)Br)F)(C(=O)N)OCCO
AZD1480	2.7	0.5	7.2	CC1=CC(=NN1)NC2=NC(=NC=C2Cl)NC(C)C3=NC=C(C(=N3)F
AZD4547	2.4	1.4	2.4	COc1cc(Cc2cc(NC(=O)c3ccc(cc3)N3C[C@H](C)N[C@H](C)C3)n[nH]2)cc(OC)c1
Volasertib	0.4	0.0	1.9	C[C@H]1N2c2nc(nc2N(C1=O)C)Nc3c(ccc3)C(C)N[C@H]4C[C@H](C4)N5CCN(CCN5CC6C6)OC(C)C(C
Cabozantinib	1.3	0.4	6.0	O=C(C1(CCN1)C(NC2=CC=C(F)C=C2)=O)NC(C=C3)=CC=C3OC4=C(C(=C(OC)C(OC)=C5)C5=NC=C4
Gefitinib	1.1	0.3	1.6	COc1cc2c(cc1OCCCN3CCOCC3)(cncn2)Nc4ccc(c(c4)Cl)F
TAK-733	0.5	0.0	0.6	CN1C2=C(C(=C(C1=O)F)NC3=C(C(=C3)I)F)C(=O)N(C(=N2)CC(CO)O
GSK2126458	0.5	-0.2	1.4	COC1=C(C(=C(N1)C2=CC3=C(C=CN=C3=C2)C4=CN=NC=C4)NS(=O)(=O)C5=C(C(=C(C5)F)F
Ibrutinib	0.6	-0.2	2.4	C=CC(=O)N1CCC[C@H](C1)N2C3=C(C(=N2)C4=CC=C(C(=C4)OC5=CC=CC=C5)C(=NC=N3)N
TAK-901	4.3	1.4	5.3	CCS(=O)(=O)C1=CC=CC(=C1)C2=CC(=C(C3=C2C4=C(C(=CN=C4N3)C)C)C(=O)NC5CCN(CCN5)C
Erlotinib	1.0	0.2	2.9	COCCOCc1cc2c(cc1OCCOC)ncnc2N3cccc(c3)C#C
GSK2636771	1.0	0.0	1.9	CC1=C(C=CC=C1(F)F)F)NC2(C=NC3=C2C=C(C(=C3C(=O)O)N4CCOCC4)C
(5Z)-7-Oxozeaenol	1.2	0.2	2.3	COc1cc(O)c2c(=O)O[C@@H](C)C(C)C=C(C(=O)[C@@H](O)[C@@H](O)C)C=C\c2c1
AZD2014	-0.1	-0.5	0.4	CC1COCCN1C2=NC(=NC3=C2C=CC(=N3)C4=CC(=CC=C4)C(=O)NC)N5CCOCC5C
Rebastinib	3.3	0.9	2.3	C(C)C1=NN(C(=C1)NC(=O)NC2=C(C(=C2)OC3=CC(=NC=C3)C(=O)NC)F)C4=C(C5=C(C(=C4)N=CC=C5
GSK269962	0.8	1.5	3.8	CCN1C2=CC(=NC=C2N=C1C3=NON=C3N)OC4=CC=CC(=C4)NC(=O)C5=CC=C(C(=C5)OCCN6CCOCC6
PF-431396	5.1	2.4	6.9	CN(C)=CC=CC=C1CNC2=NC(=NC=C2(C(F)F)F)NC3=CC4=C(C(=C3)NC(=O)C4)S(=O)(=O)C
GSK650394	2.2	0.6	1.7	C1CCC(C1)C2=C(C(=CC(=C2)C3=CC4=NC=C(C(=C34)C5=CC=CC=C5)C(=O)O
INK128	2.1	0.2	0.4	CC(C)N1C2=C(C(=N1)C3=CC4=C(C(=C3)OC(=N4

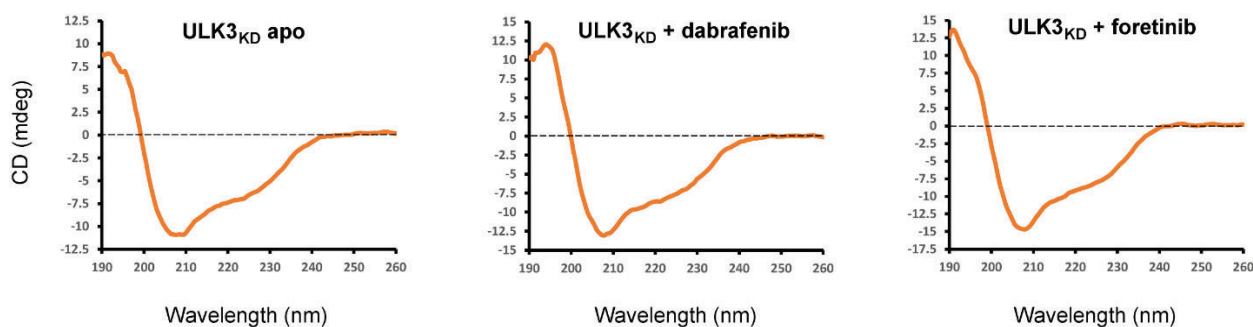
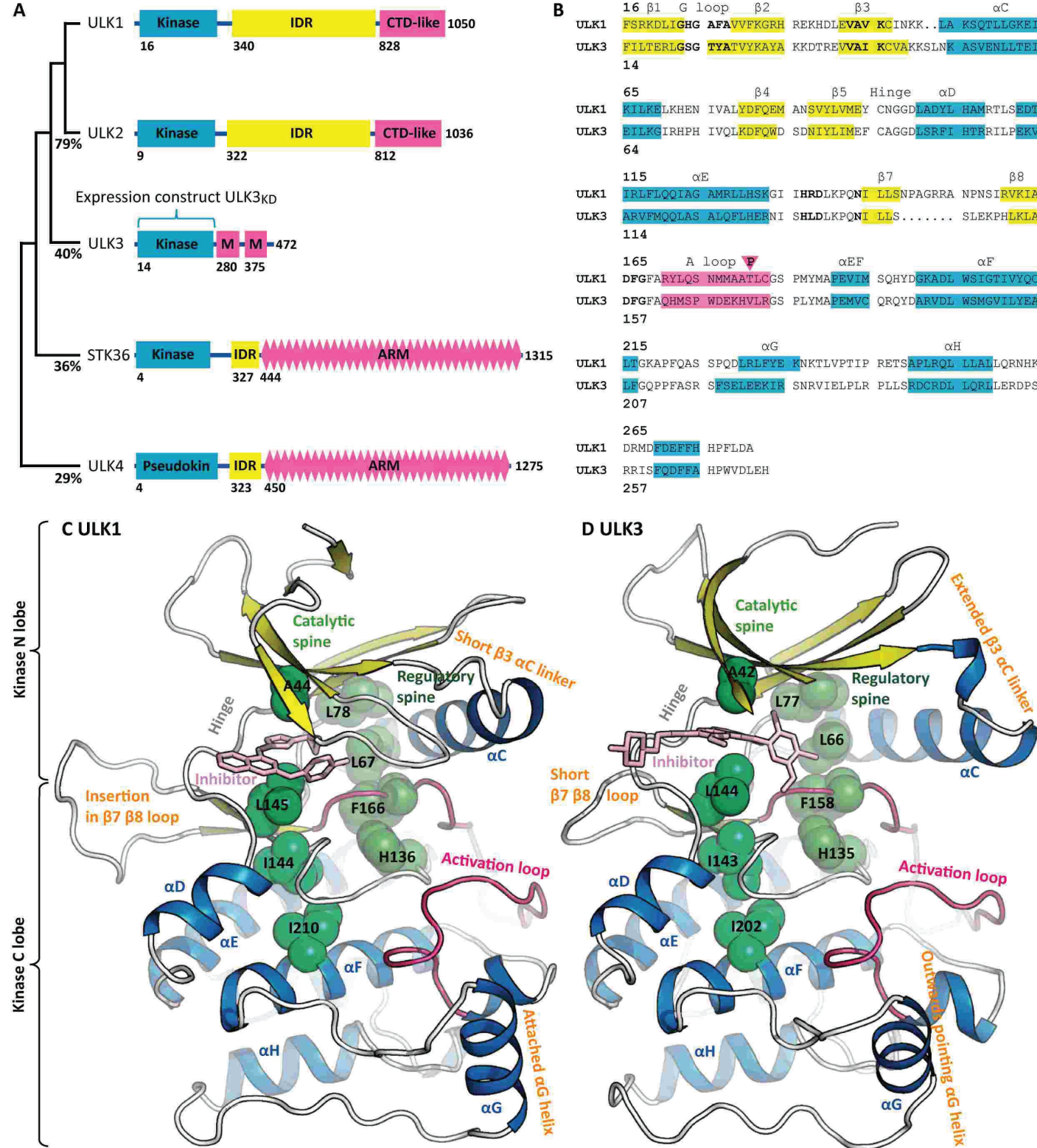
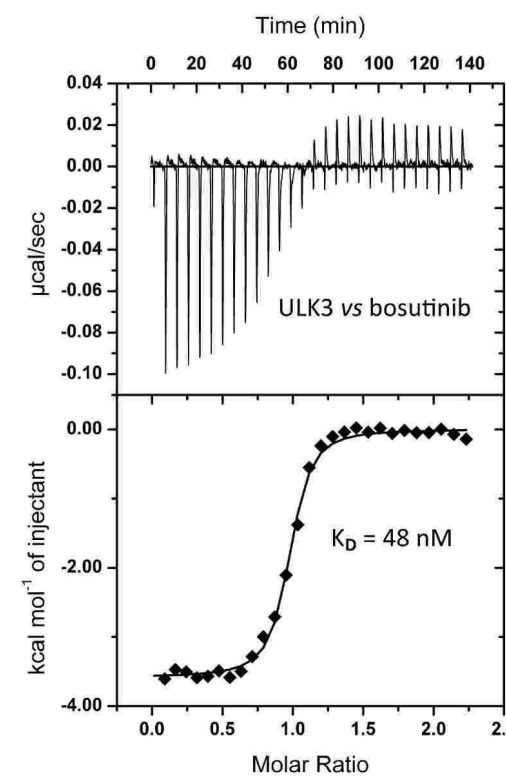
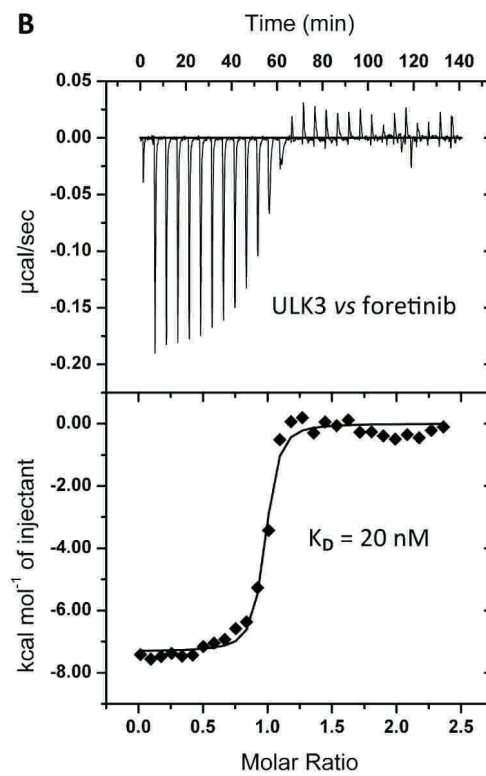
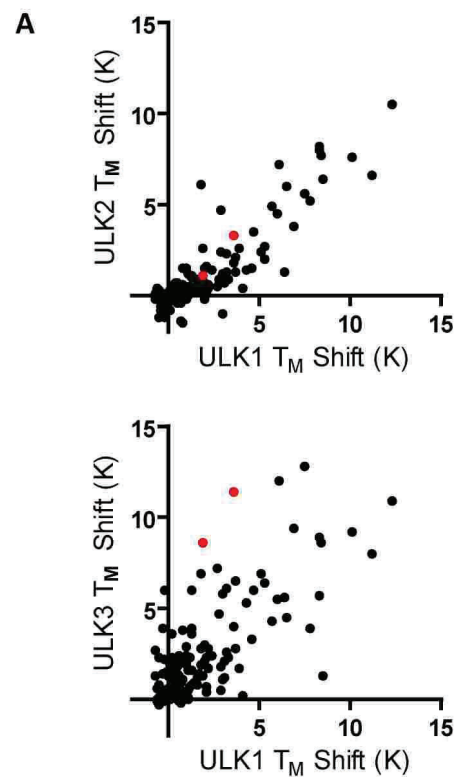


Figure S3) Circular dichroism (CD) spectra of the ULK3 kinase domain. The minima at 208 nm indicated the presence of α helices as expected for a kinase. Interestingly, no pronounced changes in secondary structure elements were induced by inhibitor binding. Subtle differences in amplitude were likely due to protein precipitation during sample preparation.

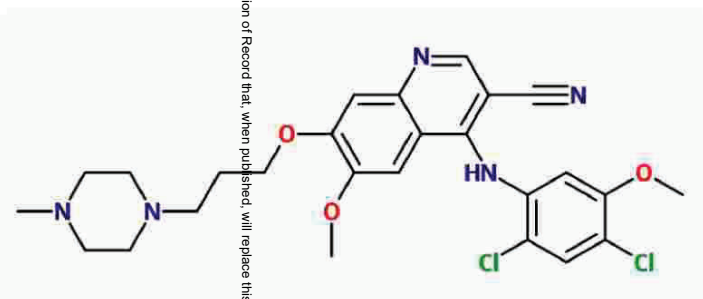




C

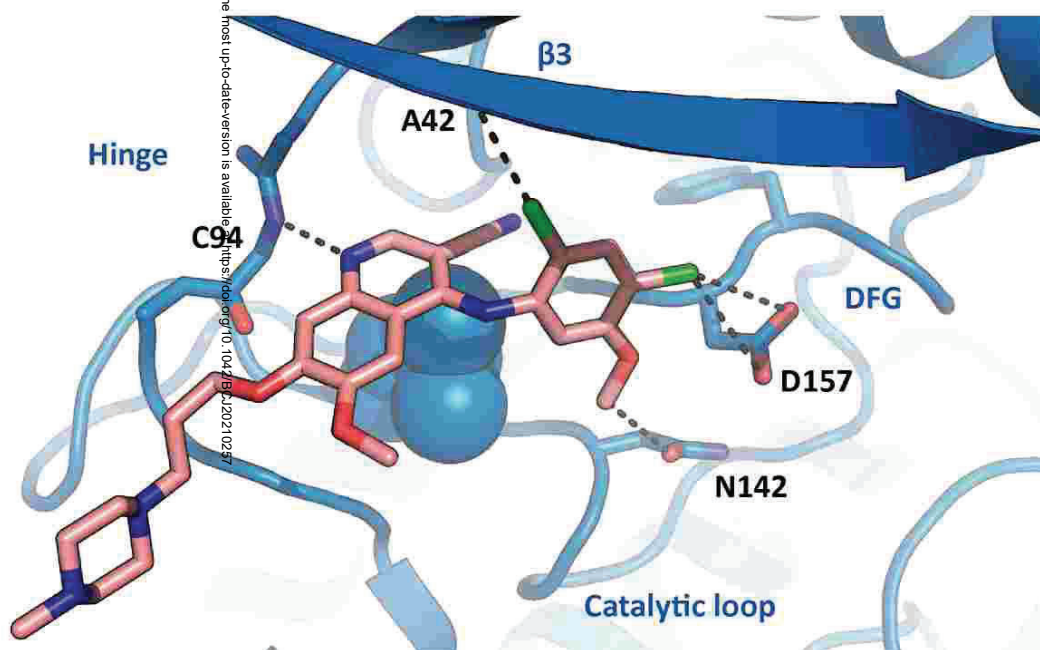
Inhibitor	T_m shift (K)			ITC K_D (nM)
	ULK1	ULK2	ULK3	
LY2874455	7.5	5.6	13	
Lestaurtinib	6.1	7.2	12	
Foretinib	3.6	3.3	11	20
Dabrafenib	12	11	11	
AT9283	6.9	3.8	9.4	
AZD7762	10	7.6	9.2	
Sunitinib	8.3	8.2	8.9	
SU6668	1.9	1.1	8.6	n.d.
PF-03758309	8.4	7.7	8.6	
AP26113	11	6.6	8.0	
AZD1480	2.7	0.5	7.2	
Nintedanib	1.8	6.1	6.9	
PF-431396	5.1	2.4	6.9	
Bosutinib	3.7	1.3	6.5	48
Momelotinib	5.3	2.4	6.4	n.d.

A Bosutinib

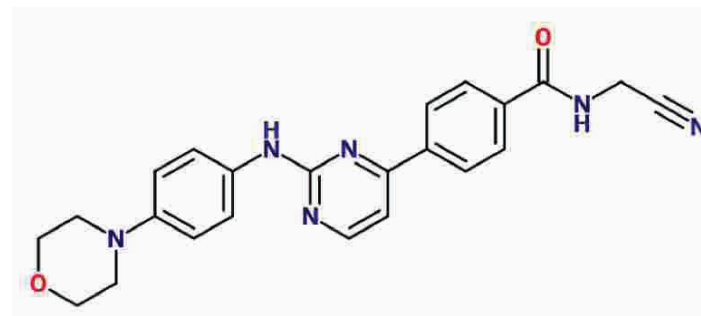


T_M shift = 6.5 K

ITC K_D = 48 nM



B Mometotinib



T_M shift = 6.4 K

ITC K_D n.d.

